Norcorrole: Aromaticity and Antiaromaticity in Contest

Peter B. Karadakov*
Department of Chemistry, University of York, Heslington, York YO10 5DD, UK

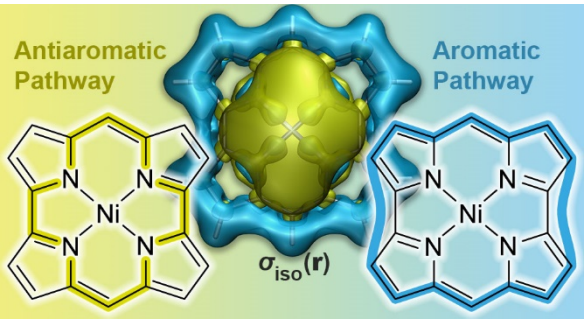

ABSTRACT: Magnetic shielding studies demonstrate that nickel norcorrole (NiNc) and norcorrole (H_2Nc) provide unusual examples of stable molecules with high antagonistic levels of antiaromaticity and aromaticity: Both incorporate an antiaromatic "core", a 14-membered cyclic conjugated subsystem with 16 π electrons, surrounded by an aromatic "halo" in the form of a ring of either 14 atoms and 14 π electrons with a new type of homoconjugation (NiNc), or 18 atoms with 18 π electrons (H_2Nc).

Aromaticity and antiaromaticity, two essential concepts deeply ingrained in chemical thinking, are usually associated with Hückel's familiar $4n + 2$ and $4n$ rules. Having both aromatic and antiaromatic behavior within the same molecule is uncommon; examples are limited to fused rings with $4n + 2$ and $4n$ π electrons such as benzocyclobutadiene[1–5] and biphenylene.[3,4,6,7] As a rule, fused $4n + 2$ and $4n$ rings both distort, leading to significant decreases of aromatic and antiaromatic character. The analysis of the isotropic magnetic shielding[8,9] enveloping Ni^{II} norcorrole (NiNc) and norcorrole (H_2Nc) shows that these molecules provide unusual examples of conjugated systems with high antagonistic levels of antiaromaticity and aromaticity. Norcorrole, the smallest cyclic tetrapyrrole porphyrin analogue synthesized to date,[10,11] was initially proposed on the basis of DFT calculations.[12] The contraction of porphyrin through removal of one meso-methine unit results in corrole; further contraction, through removal of a second meso-methine unit, produces norcorrole (H_2Nc). Although NiNc has been found to be reasonably stable,[11] both experiment and theory indicate that this complex has certain antiaromatic features. Experimental evidence of antiaromatic behavior comes from the NiNc ^{1}H NMR and MCD spectra;[11] on the theory side, antiaromaticity is suggested by DFT-level NICS, HOMA values, ACID plots, out-of-plane bond magnetizabilities and magnetically induced current densities.[11,13-16] NiNc units have been used in the construction of "an antiaromatic-walled nanospace".[17] In contrast to other antiaromatic species, such as the classical example of antiaromaticity, cyclobutadiene, C_4H_4, NiNc does not undergo a 2nd-order Jahn-Teller transition lowering the energy, reducing the symmetry and introducing bond length alternation (in the case of C_4H_4, from square D_{4h} to rectangular D_{2h}). Instead, DFT results[15] show that the highest-symmetry geometry of NiNc, planar D_{2h}, corresponds to the transition state (TS) for a bowl-to-bowl inversion connecting two equivalent shallow bowl-shaped geometries of C_{2v} symmetry with not much in the way of bond length alternation, which are just 0.7 kcal mol^{-1} lower in energy. The reason why NiNc behaves so differently from other antiaromatic molecules has been attributed to the high stability of the dipyrrin fragments, assumed to retain their electronic and structural integrity within the norcorrole ring system.[15] While this model accounts for some of the features of bonding in norcorrole, it does not explain what holds the two dipyrrin fragments together and why the C_α–C_α bonds between these fragments are long and readily oxidized.[11] The variations in isotropic magnetic shielding around NiNc and H_2Nc shows that bonding in these systems is even more unusual and intriguing than previously thought and involves an antiaromatic "core" surrounded by an aromatic outer ring which, in NiNc, features a new type of homoconjugation over the C_α–C_α bonds.

The isotropic magnetic shielding, $\sigma_{iso}(\mathbf{r}) = \frac{1}{3}[\sigma_{xx}(\mathbf{r}) + \sigma_{yy}(\mathbf{r}) + \sigma_{zz}(\mathbf{r})]$, can be calculated at any point $\mathbf{r}$ in the space surrounding a molecule; differences between $\sigma_{iso}(\mathbf{r})$ values at nuclei correspond to experimentally measurable NMR shifts. 3D grids of $\sigma_{iso}(\mathbf{r})$ values computed at the B3LYP-GIAO/6-311++G(d,p) level were employed to construct NiNc and H_2Nc $\sigma_{iso}(\mathbf{r})$ isosurfaces (Figure 1). For the purposes of this study, the ground state potential energy surfaces (PES) of NiNc and H_2Nc in the gas phase were investigated at the B3LYP-D3BJ/def2-TZVP level. In addition to the C_{2v} local minimum and planar D_{2h} TS geometries of NiNc, and the C_i local minimum geometry of H_2Nc, for which the current results agree very well with those reported previously,[15] two further stationary points on the H_2Nc PES were located, a bowl-shaped C_2 local minimum and a planar C_{2h} 2nd-order saddle point; these last have not been reported in the literature. The C_{2h} 2nd-order saddle point acts as TS for both the bowl-to-bowl inversion between two equivalent C_2 local minima and the flip between two equivalent C_i local minima. The C_2 and C_i geome-

tries of H_2Nc were found to be 2.10 and 2.04 kcal mol^{-1}, respectively, lower in energy than the C_{2h} 2nd-order saddle point. The H_2Nc PES analysis was repeated with a second DFT method, PBE0-D3BJ/def2-TZVP. With this method, the C_2 and C_i geometries of H_2Nc were found to be 1.37 and 1.57 kcal mol^{-1}, respectively, lower in energy than the C_{2h} 2nd-order saddle point. These small energy differences suggest that the C_2 and C_i geometries of H_2Nc can easily interconvert in the gas phase through the C_{2h} 2nd-order saddle point; thorough examination of the H_2Nc PES indicates that there is no TS linking these geometries directly. The flatter C_i geometry is preferred in the solid state and in solution.[14] A better estimate of the experimentally observed Ni–C distance in NiNc (1.771 Å to 1.789 Å[15]) was obtained at the TPSSh-D3BJ/def2-TZVP level, 1.796 Å against 1.810 Å at the B3LYP-D3BJ/def2-TZVP level.

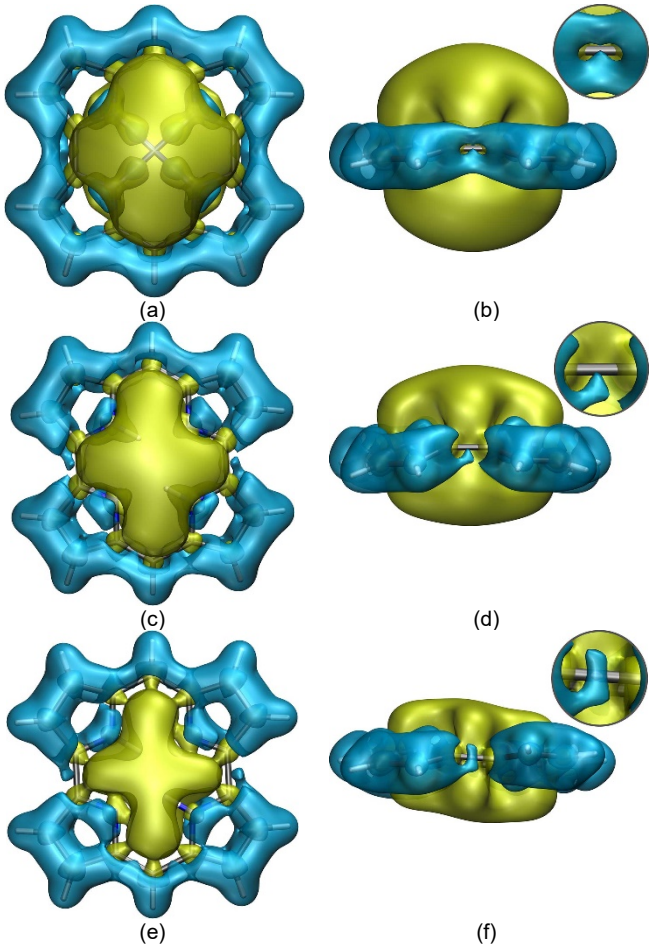

Figure 1. Shielding around NiNc and H_2Nc. Isosurfaces at $\sigma_{iso}(\mathbf{r})$ = +12 ppm (aromatic regions, blue) and $\sigma_{iso}(\mathbf{r})$ = −12 ppm (antiaromatic regions, yellow). (a, b) NiNc top and side views; H_2Nc: C_2 (c, d) and C_i (e, f) geometries, top and side views. Magnified sections in (b, d, f) show C_α–C_α bonds.

Before discussing the NiNc and H_2Nc $\sigma_{iso}(\mathbf{r})$ isosurfaces (Figure 1), it is instructive to examine shielding around benzene and cyclobutadiene (C_6H_6 and C_4H_4, Figure 2, at D_{6h} and D_{2h} optimized geometries, same levels of theory as for for NiNc and H_2Nc). The benzene ring is enclosed within a thick shielded "doughnut" which demonstrates strong bonding interactions and aromatic stability. Antiaromatic destabilization in C_4H_4 follows from the central deshielded region which eliminates most of the shielding over C–C "single" bonds and pushes "double" bonds towards the exterior of the ring, weakening both types of bond, albeit to somewhat different extents. While the isosurfaces in Figure 2 are qualitatively similar to those obtained previously at other levels of theory,[8,9] it should be noted that rectangular (D_{2h}) C_4H_4 is considerably less antiaromatic than square (D_{4h}) C_4H_4.[18,19] As shown previously,[20,21] $\sigma_{iso}(\mathbf{r})$ is capable of exposing the differences between bonds of different strengths in much greater detail than is achievable using the total electronic density. The isovalues $\sigma_{iso}(\mathbf{r})$ = +12 ppm were chosen so as to show optimal levels of detail in Figures 1 and 2. Isosurfaces for other isovalues can be inspected using the Gaussian cube files provided in the Supporting Information.

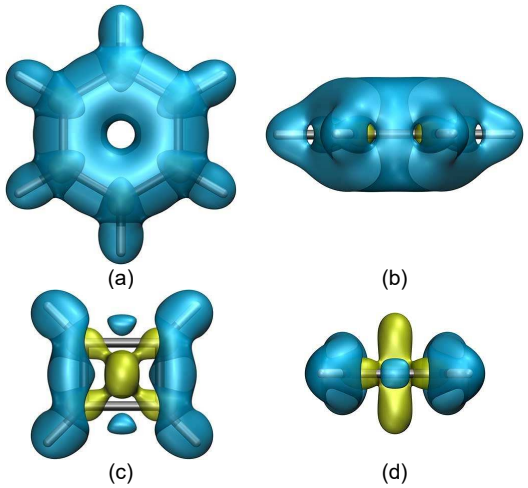

Figure 2. Shielding around C_6H_6 and C_4H_4. Top and side views: (a, b) C_6H_6, (c, d) C_4H_4. Isosurface details as in Figure 1.

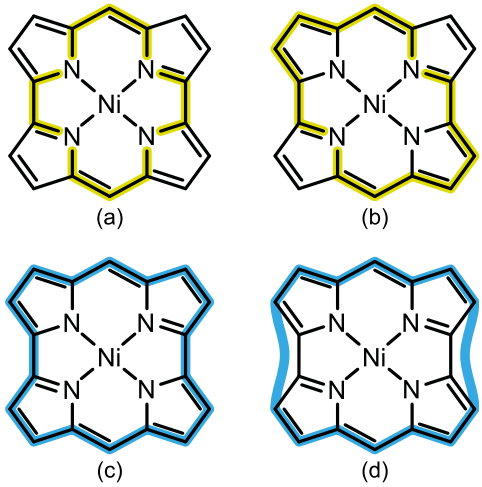

Figure 3. Conjugation pathways in NiNc. (a) antiaromatic, 14 atoms and 16 π electrons (this work); (b) antiaromatic, 16 atoms and 16 π electrons[11,12–14] (c, d) aromatic, 18 atoms and 18 π electrons, or 14 atoms and 14 π electrons (this work).

Both NiNc and H_2Nc feature central deshielded regions resembling that in C_4H_4 but considerably larger in size (Figure 1). These regions extend over a 14-membered cyclic conjugated subsystem with 16 π electrons (Figure 3(a)) which is more compact than the 16-membered conjugated circuit with the same number of π electrons (Figure 3(b)) hitherto thought to be the source of antiaromatic character in norcorrole.[11,12,14] The view that the antiaromaticity of NiNc follows from the pathway in Figure 3(b) has not been challenged previously, although evidence that the pathway in Figure 3(a) provides the more realistic option has been hiding in plain sight. Large magnetically induced current densities over the pathway in Figure 3(a) were observed in previous studies of NiNc[15] and Ni^{II} cyanonorcorrole[16]; a NICS contour plot for a NiNc derivative[22] akin to a planar slice through the surface in Figure 1(a, b) shows deshielding beneath the area of this pathway; it has been argued that in ACID plots for substituted NiNc the main

ring current "flows along the inner periphery involving four nitrogen atoms and fourteen bonds"[23,24] although inspection of these ACID plots shows significant paratropic currents all over the NiNc unit. The antiaromatic pathway in NiNc (Figure 3(a)) resembles an antiaromatic pathway with 16 atoms and 16 π electrons in the octaethylporphyrin Zn^{II} dication,[25] established through DFT GIMIC[26] calculations; the absence of two meso-methine units in neutral NiNc produces the same 16 π electron count as that in the octaethylporphyrin Zn^{II} dication.

Nickel enhances the antiaromaticity of the central region in NiNc, most likely by creating additional conjugation pathways. To check if Ni contributes electrons to the π system, natural population analyses (NPA) were carried out at the level of theory used in the geometry optimizations. The NPA charge on Ni was obtained as 0.470*e* and the NPA charge distributions in NiNc and H_2Nc turned out to be reasonably similar (Figure S2). Thus, the Ni contribution to the NiNc π system is minor and does not need to be taken into account in π electron counts. The shielded ovoids between Ni and N atoms (Figure 1(a)) provide evidence of Ni–N bonding; despite their relatively small sizes, shielding within these ovoids reaches values of over 72 ppm. The effect of the central deshielded regions in NiNc and H_2Nc on C–N and C–C bonds is similar to that observed in C_4H_4 (Figure 2(c, d)) but, surprisingly, none of the bonds along the NiNc perimeter are affected as much as the C_4H_4 "single" bonds. In fact, the antiaromatic "core" in NiNc is surrounded by a shielded 18-membered ring with 18 π electrons which, despite the two "weaker" links across C_α–C_α bonds, suggests well-established bonding interactions. While a conjugated ring with 18 π electrons (Figure 3(c)) can be considered as Hückel-aromatic, it is apparent that the level of aromatic stabilization of the ring surrounding NiNc is lower than that of C_6H_6 (Figure 2(a, b)). A closer look at the shielding around the C_α–C_α bonds reveals additional details: The distancing of the $\sigma_{iso}(\mathbf{r})$ = 12 ppm isosurface from these bonds (Figure 1(a)) and the apertures in the isosurface (Figure 1(b)) suggest that the conjugated "halo" around NiNc is bypassing the *α* carbons, preferring through-space conjugation similar to homoconjugation[27–29] between the *β* carbons instead. With homoconjugation, the conjugated ring around the perimeter of NiNc is reduced to 14 atoms and 14 π electrons (Figure 3(d)) and remains Hückel-aromatic. In this way, the shielding around the C_α–C_α bonds identifies these bonds as the weakest and most reactive along the NiNc outer perimeter.[11] Similarly to NiNc, the deshielded central region in H_2Nc involves a 14-membered circuit with 16 π electrons but its smaller size and different shape indicate weaker antiaromatic character. In this case, shielding along the outer frame outlines two interacting dipyrrin fragments with much less if any homoconjugation across the links between these fragments. Of course, a lower isovalue for H_2Nc, say $\sigma_{iso}(\mathbf{r})$ = ±10 ppm, would produce a positive $\sigma_{iso}(\mathbf{r})$ isosurface enveloping the C_α–C_α bonds to a greater extent. The central antiaromatic region in the bowl-shaped H_2Nc geometry of C_2 symmetry is larger and closer in size and shape to that in NiNc.

NICS(0)[3] and NICS(1),[30,31] which measure $-\sigma_{iso}$(at ring center) and $-\sigma_{iso}$(at 1 Å above ring center), respectively, provide a more conventional way of estimating aromaticity in NiNc and H_2Nc. A complication arises from the fact that both molecules are non-planar. Calculating NICS(0) is less of a problem because the center of a non-planar ring can be located by averaging the coordinates of its atoms; NICS(0) values have been reported for some norcorrole derivatives.[11,14,22-24] One way of defining NICS(1) positions for non-planar rings is to fit a plane to the ring atoms and ring center, and then use the points 1 Å above and below along the normal passing through the ring centre.[32] In general, these two points are not equivalent by symmetry and give different NICS(±1) values. B3LYP-GIAO and PBE0-GIAO NICS(0), NICS(1) and nuclear isotropic shielding values for C_6H_6 and C_4H_4 are shown in Figure S3. Analogous information for NiNc and H_2Nc, with the addition of NICS(−1) values, is shown in Figure S4. Whereas the choice of DFT method affects Ni, N and C nuclear shieldings, related changes in proton and off-nucleus shieldings, such as NICS and shielding isosurfaces (Figures 1 and 2) are much more minor. The NICS(0) and NICS(±1) values calculated within the central 14-membered circuits with 16 π electrons in NiNc and H_2Nc confirm that the interior of NiNc is significantly more antiaromatic than that of H_2Nc; the level of antiaromaticity in the interior of H_2Nc at the C_i geometry is close to that in C_4H_4 (Figures S3 and S4). The NICS(0) and NICS(±1) values for the pyrrole rings in NiNc are negative but of relatively low magnitudes; the corresponding values for the pyrrole rings in H_2Nc are a mixture of positive and negative numbers of even lower magnitudes. These observations suggest that in both NiNc and H_2Nc the individual pyrrole rings should be considered as non-aromatic. Clearly, while NICS can be used to identify the antiaromatic features of NiNc and H_2Nc, these indices are unable to spot the presence of the aromatic "halos" surrounding these molecules. A detail worth drawing attention to is the very substantial deshielding of the two hydrogens in the interior of H_2Nc (Figure S4(c–f)), which is a consequence of the positioning of these hydrogens inside the central deshielded region of this molecule (Figure 1(c, e)) and has been observed experimentally.[14] Not coincidentally, these "inner" hydrogens have high positive NPA charges (Figure S2(b, c)).

As shown in this communication, through a visual approach in which bonding and aromaticity can be inspected using 3D isotropic magnetic shielding isosurfaces, norcorrole combines a strongly antiaromatic interior with an aromatic "halo" along its outer perimeter, providing a unusual example of a stable molecule in which aromaticity and antiaromaticity coexist in balance. This description of norcorrole provides an exception to the notion that the stability of porphyrinoids follows from "appended 6π electronic sextets":[33] As shown in Figure 1, the large deshielded region in the center of norcorrole disrupts the shielding within pyrrole rings and makes them non-aromatic; this is also supported by the NICS(0) and NICS(±1) values for these rings. It has been emphasized,[18,19,34] that the proper description of the magnetic properties of antiaromatic molecules requires the use of CASSCF wavefunctions as such molecules often exhibit significant open-shell singlet character. Computational evidence indicates that the antiaromaticity of rectangular (D_{2h}) cyclobutadiene is overestimated by methods based on closed-shell wavefunctions such as HF, MP2 and B3LYP.[18,19] However, a CASSCF-GIAO calculation on NiNc in an active space large enough to take into account all conjugation pathways is not feasible at present, as the size of this active space is well beyond the capabilities of current codes. Were it possible to do such a calculation, the central antiaromatic region would become smaller while the aromatic "halo" would expand, enhancing the aromatic stabilization of this molecule and lending further support to the description suggested in this communication.

ASSOCIATED CONTENT

Supporting Information.

The Supporting Information is available free of charge at http://pubs.acs.org.

Figures showing bond lengths in the local minimum geometries of NiNc and H_2Nc; NPA charges for NiNc and H_2Nc; NICS values and isotropic shieldings for benzene, cyclobutadiene, NiNc and H_2Nc; computational details including optimized geometries; additional references (PDF). Zip archive of Gauss-

ian cube files with isotropic shielding values for benzene, cyclobutadiene, NiNc and H_2Nc (ZIP).

AUTHOR INFORMATION

Corresponding Author

Peter B. Karadakov — *Department of Chemistry, University of York, Heslington, York YO10 5DD, UK;* ORCID orcid.org/0000-0002-2673-6804; Email: peter.karadakov@york.ac.uk

REFERENCES

(1) Winter, W.; Straub, H. Molecular structure of a benzocyclobutadiene. *Angew. Chem. Int. Ed. Engl.* **1978**, *17*, 127–128.

(2) Karadakov, P. B.; Gerratt, J.; Cooper, D. L.; Raimondi, M.; Sironi, M. Modern valence-bond description of the electronic structure of benzocyclobutadiene. *Int. J. Quantum Chem.* **1996**, *60*, 545–552.

(3) Schleyer, P. v. R.; Maerker, C.; Dransfeld, A.; Jiao, H.; van Eikema Hommes, N. J. R. Nucleus-independent chemical shifts: A simple and efficient aromaticity probe. *J. Am. Chem. Soc.* **1996**, *118*, 6317–6318.

(4) McKee, M. L.; Balci, M.; Kilic, H.; Yurtsever, E. Computational studies of cyclobutadiene and benzocyclobutene fused to *p*- and *o*-quinone. *J. Phys. Chem. A* **1998**, *102*, 2351–2356.

(5) Jensen, M. Ø.; Thorsteinsson, T.; Hansen, A. E. Benzocyclobutadiene: The question of structures, magnetic shieldings, and aromatic character. *Int. J. Quantum Chem.* **2002**, *90*, 616–628.

(6) Pagano, J. K.; Xie, J.; Erickson, K. A.; Cope, S. K.; Scott, B. L.; Wu, R.; Waterman, R.; Morris, D. E.; Yang, P.; Gagliardi, L.; Kiplinger, J. L. Actinide 2-metallabiphenylenes that satisfy Hückel's rule. *Nature* **2020**, *578*, 563–576.

(7) Gantenbein, M.; Li, X.; Sangtarash, S.; Bai, J.; Olsen, G.; Alqorashi, A.; Hong, W.; Lambert, C. J.; Bryce, M. R. Exploring antiaromaticity in single-molecule junctions formed from biphenylene derivatives. *Nanoscale* **2019**, *11*, 20659–20666.

(8) Karadakov, P. B.; Horner, K. E. Magnetic shielding in and around benzene and cyclobutadiene: A source of information about aromaticity, antiaromaticity and chemical bonding. *J. Phys. Chem. A* **2013**, *117*, 518–523.

(9) Karadakov, P. B.; Hearnshaw, P.; Horner, K. E. Magnetic shielding, aromaticity, antiaromaticity, and bonding in the low-lying electronic states of benzene and cyclobutadiene. *J. Org. Chem.* **2016**, *81*, 11346–11352.

(10) Bröring, M.; Köhler, S.; Kleeberg, C. Norcorrole: Observation of the smallest porphyrin variant with a N_4 core. *Angew. Chem. Int. Ed.* **2008**, *47*, 5658–5660.

(11) Ito, T.; Hayashi, Y.; Shimizu, S.; Shin, J.-I.; Kobayashi, N.; Shinokubo, H. Gram-scale synthesis of nickel(II) norcorrole: The smallest antiaromatic porphyrinoid. *Angew. Chem. Int. Ed.* **2012**, *51*, 8542–8545.

(12) Ghosh, A.; Wasbotten, I. H.; Davis, W.; Swarts, J. C. Norcorrole and dihydronorcorrole: A predictive quantum chemical study. *Eur. J. Inorg. Chem.* **2005**, 4479–4485.

(13) Nozawa, R.; Tanaka, H.; Cha, W.-Y.; Hong, Y.; Hisaki, I.; Shimizu, S.; Shin, J.-Y.; Kowalczyk, T.; Irle, S.; Kim, D.; Shinokubo, H. Stacked antiaromatic porphyrins. *Nat. Comm.* **2016**, *7*, 13620(1–7).

(14) Yonezawa, T.; Shafie, S. A.; Hiroto, S.; Shinokubo, H. Shaping antiaromatic π-aystems by metalation: Synthesis of a bowl-shaped antiaromatic palladium norcorrole. *Angew. Chem. Int. Ed.* **2017**, *56*, 11822–11825.

(15) Conradie, J.; Foroutan-Nejad, C.; Ghosh, A. Norcorrole as a delocalized, antiaromatic system. *Sci. Rep.* **2019**, *9*, 4852(1–6).

(16) Fliegl, H.; Valiev, R; Pichierri, F.; Sundholm, D. Theoretical studies as a tool for understanding the aromatic character of porphyrinoid compounds *Chem. Modell.* **2018**, *14*, 1–42.

(17) Yamashina, M.; Tanaka, Y.; Lavendomme, R.; Ronson, T. K.; Pittelkow, M.; Nitschke, J. R. An antiaromatic-walled nanospace. *Nature* **2019**, *574*, 511–515.

(18) Karadakov, P. B. Ground- and excited-state aromaticity and antiaromaticity in benzene and cyclobutadiene. *J. Phys. Chem. A* **2008**, *112,* 7303–7309.

(19) Pathak, S.; Bast, R.; Ruud, K. Multiconfigurational self-consistent field calculations of the magnetically induced current density using gauge-including atomic orbitals. *J. Chem. Theory Comput.* **2013**, *9*, 2189–2198.

(20) Karadakov, P. B.; Horner, K. E. Exploring chemical bonds through variations in magnetic shielding. *J. Chem. Theory Comput.* **2016**, *12*, 558–563.

(21) Karadakov, P. B.; Kirsopp, J. Magnetic shielding studies of C_2 and C_2H_2 support higher than triple bond multiplicity in C2 *Chem. Eur. J.* **2017**, *23*, 12949–12954.

(22) Nozawa, R,; Kim, J.; Oh, J.; Lamping, A.; Wang, Y.; Shimizu, S.; Hisaki, I.; Kowalczyk, T.; Fliegl, H.; Kim, D.; Shinokubo, H. Three-dimensional aromaticity in an antiaromatic cyclophane. *Nat. Comm.* **2019**, *10*, 3576(1–7).

(23) Nozawa, R.; Yamamoto, K.; Hisaki, I.; Shina, J.-Y.; Shinokubo, H. Ni^{II} tetrahydronorcorroles: antiaromatic porphyrinoids with saturated pyrrole units. *Chem. Commun.* **2016**, *52*, 7106–7109.

(24) Yoshida, T.; Takahashi, K.; Ide, Y.; Kishi, R.; Fujiyoshi, J.-Y.; Lee, S.; Hiraoka, Y.; Kim, D.; Nakano, M.; Ikeue, T.; Yamada, H.; Shinokubo, H. Benzonorcorrole Ni^{II} complexes: Enhancement of paratropic ring current and singlet diradical character by benzofusion. *Angew. Chem. Int. Ed.* **2018**, *57*, 2209–2213.

(25) Fliegl, H.; Pichierri, F.; Sundholm, D. Antiaromatic character of 16 π electron octaethylporphyrins: Magnetically induced ring currents from DFT-GIMIC calculations. *J. Phys. Chem. A* **2015**, *119*, 2344–2350.

(26) Fliegl, H.; Taubert, S.; Lehtonen, O.; Sundholm, D. The gauge including magnetically induced current method. *Phys. Chem. Chem. Phys.* **2011**, *13*, 20500–20518.

(27) Williams, R. V. Homoaromaticity. *Chem. Rev.* **2001**, *101*, 1185–1204.

(28) Fliegl, H.; Sundholm, D.; Taubert, S.; Jusélius J.; Klopper W. Magnetically induced current densities in aromatic, antiaromatic, homoaromatic, and nonaromatic hydrocarbons. *J. Phys. Chem. A* **2009**, *113*, 8668–8676.

(29) Karadakov, P. B.; Cooper, D. L. Modern valence-bond description of homoaromaticity. *J. Phys. Chem. A* **2016**, *120*, 8769–8779.

(30) Schleyer, P. v. R.; Jiao, H.; van Eikema Hommes, N. J. R.; Malkin, V. G.; Malkina, O. An evaluation of the aromaticity of inorganic rings: refined evidence from magnetic properties. *J. Am. Chem. Soc.* **1997**, *119*, 12669–12670.

(31) Fallah-Bagher-Shaidaei, H.; Wannere, C. S.; Corminboeuf, C.; Puchta, R.; Schleyer, P. v. R. Which NICS aromaticity index for planar π rings is best? *Org. Lett.* **2006**, *8*, 863–866.

(32) Dobrowolski, J. Cz.; Lipiński, P. F. J. On splitting of the NICS(1) magnetic aromaticity index. *RSC Adv.* **2016**, *6*, 23900–23904.

(33) Wu, J. I.; Fernández, I.; v. R. Schleyer, P. Description of aromaticity in porphyrinoids. *J. Am. Chem. Soc.* **2013**, *135*, 315–321.

(34) Karadakov, P. B. Aromaticity and antiaromaticity in the low-lying electronic states of cyclooctatetraene. *J. Phys. Chem. A* **2008**, *112*, 12707–12713.